Tunable emission from localized excitons deterministically positioned in monolayer p–n junctions

Erik J. Lenferink,[†] Trevor LaMountain,[‡] Teodor K. Stanev,[†] Ethan Garvey,[†] Kenji Watanabe,[¶] Takashi Taniguchi,[§] and Nathaniel P. Stern[*,†]

[†]*Department of Physics and Astronomy, Northwestern University, Evanston, Illinois 60208, USA*

[‡]*Applied Physics Program, Northwestern University, Evanston, Illinois 60208, USA*

[¶]*Research Center for Functional Materials, National Institute for Materials Science, 1-1 Namiki, Tsukuba 305-0044, Japan*

[§]*International Center for Materials Nanoarchitectonics, National Institute for Materials Science, 1-1 Namiki, Tsukuba 305-0044, Japan*

E-mail: n-stern@northwestern.edu

Abstract

Transition metal dichalcogenides (TMDs) are a promising solid-state platform for single photon emission. The versatile fabrication methods afforded by their two-dimensional nature facilitate the integration of TMDs into optoelectronic devices where localized exciton states can be electrically pumped. While this functionality is highly desirable for applications in quantum nanophotonics, enabling more compact and scalable devices, the lack of control of emitter spatial positions and energies has impeded the integration of TMDs into quantum optical systems. Here we demonstrate single

photon electroluminescence from monolayer WSe_2 in a lateral gate-defined junction that allows the electrostatic environment to be tuned *in situ*. By utilizing local strain engineering, we reliably position bright localized exciton states in the optically active region of the gate-defined junction, enabling the deterministic creation of devices which predominantly produce single photon emission. Modulation of the gate voltages tunes the emission between different electrostatic regimes, revealing a new localized exciton state which exhibits a gate-dependent redshift. A spectral shift of the electroluminescence of over 10 meV is achieved, demonstrating the capability for simultaneous electrical pumping and tuning of localized exciton emission in TMD devices.

Keywords

two-dimensional materials, single-photon emitter, electroluminescence, p-n junction, lateral device

Introduction

Single photon emitters (SPEs) are an essential component for a number of emerging technologies based on the photon nature of light such as quantum information processing and quantum cryptography.[1,2] While SPE behavior appears in many physical systems including atoms and molecules[3–6] solid-state sources such as quantum dots[7] and color centers in diamond[8] are well-suited for applications in quantum nanophotonics as they provide the mechanisms for tuning in devices through control of composition, structure, and externally applied fields. More critically, the compatibility of solid-state sources with standard nanofabrication processes enables the creation of optoelectronic devices where SPEs can be electrically pumped. This is highly desirable for quantum nanophotonics as it facilitates more scalable and compact devices by removing the need for separate optical pumping, opening the door to quantum information processing on an optical chip.[9–14]

New opportunities for the electric control of solid-state SPEs have emerged with the discovery of single photon emission in two-dimensional layered materials including transition metal dichalcogenides (TMDs) and boron nitride originating from exciton states strongly localized to random crystal defects.[15–21] Due to the weak van der Waals forces between layers, optoelectronic devices may be engineered layer-by-layer from these materials using polymer-based transfer methods,[22,23] opening up an entirely new fabrication route for electrically-pumped SPEs. Exemplifying this, electroluminescence (EL) from monolayer TMD SPEs was demonstrated in two distinct types of devices created with these transfer methods: vertical tunneling devices, in which a current is injected into the monolayer from top and bottom graphene terminals,[24–26] and lateral p–n junctions, in which metal contacts inject a lateral current between p- and n-type regions of the monolayer defined by local gates.[24]

While these devices mark a significant step towards the integration of electrically-pumped TMD SPEs into quantum nanophotonics, several issues limit their scalability. Specifically, the reliance on natural crystal defects means that the fabrication process is highly stochastic: a device will have an indeterminate number of SPEs distributed randomly over the monolayer area with emission energies that are highly variable due to local inhomogeneities.[15–20] For practical scalable quantum devices, control of SPE positions and energies is necessary to efficiently couple their emission to photonic nanostructures.[27–29] Recently the use of local strain engineering has been demonstrated to enable the deterministic creation of bright localized exciton states in the vertical device structure with sub-micrometer accuracy,[30] however the emission energies are still effectively random despite efforts to precisely engineer the strain profile.[31–33] In order for TMD SPEs to be viable in applications such as optical quantum computation where the indistinguishably of SPEs is critical,[34,35] post-fabrication, *in situ* control of emission energies is essential.

One promising means to achieve this is to utilize electrostatic gating which has been shown in photoluminescence (PL) studies of TMDs to activate localized trion states[36–38] and induce Stark shifts of localized excitons over several meV.[26,39–41] Accomplishing similar

control of the EL is an additional challenge, requiring independent control of the injection current (which pumps SPEs) and gate fields (which determine the emission properties).[42] Of the two types of TMD devices used to produce EL from SPEs, only the gate-defined lateral p–n junction satisfies this condition: by modulating the gate voltages while applying a constant lateral current, the charge density and fields in the junction can be tuned,[43] in principle enabling electrical tuning of the SPE EL. The key hurdle for accomplishing this has been positioning bright localized exciton states in the narrow junction region. To date, SPE EL has only been reported from a single gate-defined device.[24]

In this report we utilize local strain engineering to reliably produce SPE EL from gate-defined lateral p–n junctions based on monolayer WSe_2. Similar to recent work which studied the spectral photoresponse of TMD-based lateral p–n junctions,[44] high strain gradients are created in the narrow junction region of devices by embedding dielectric nanopillars under the WSe_2, enabling efficient funneling of charge carriers into bright localized excitons.[32,33] This yields a deterministic method for creating gate-defined p–n junctions which predominantly emit antibunched EL with little polluting nonlocalized emission. By tuning the electrostatic environment in the junctions into the strongly n-gated regime, a novel species of localized excitons which exhibits a gate-dependent redshift is observed. Selective modulation of the gate voltages induces spectral shifts of the EL over 10 meV, demonstrating significant progress towards integrating a tunable solid-state single photon source into a scalable quantum optoelectronic device.

Results and Discussion

Demonstration of SPE electroluminescence

The fabrication process employed here to produce SPE EL in monolayer devices, illustrated in Fig. 1a, largely follows the same procedures previously utilized to create gate-defined p–n junctions from TMDs[43,45–48] but with one key difference: the addition of a dielectric

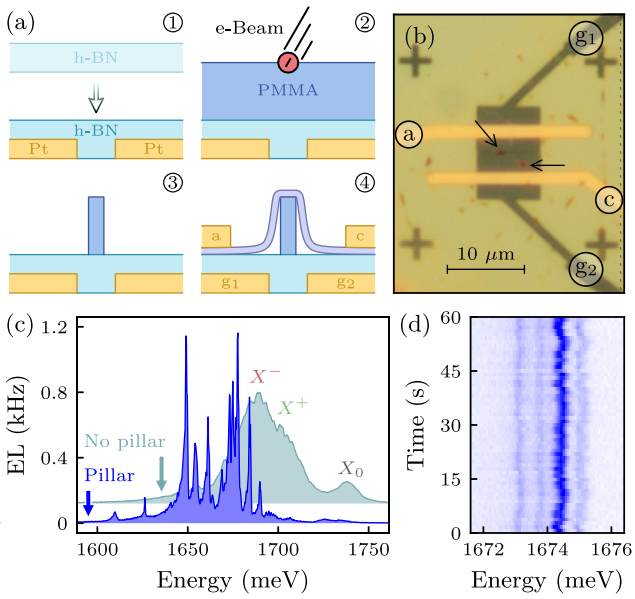

Figure 1: **Realization of localized exciton electroluminescence using strain engineering. (a)** Illustration of the fabrication process: (1) a h-BN flake is transferred onto two bottom gates; (2) PMMA is spun on top and irradiated at a high dosage; (3) the PMMA is dissolved, leaving a nanopillar; (4) a WSe_2 flake is transferred on top and contacts are created. **(b)** Optical microscopy image of an example monolayer WSe_2 p–n junction device with two nanopillar strain sites (denoted by arrows), one of which migrated away from the central junction during fabrication. Dotted lines represent the edges of the monolayer. **(c)** EL spectrum of a monolayer WSe_2 nanopillar p–n junction device with an injection current of 4.5 nA (blue). A typical low-temperature (4 K) EL spectrum of an unstrained device (teal) is also shown, not to scale. **(d)** High-resolution EL spectra collected over the course of one minute of a bright doublet for the strained device in (c). A second, lower-intensity doublet can also be seen.

nanopillar to function as a strain site.[32,33] The process begins with the creation of two bottom gates, laterally separated by a distance of 300 nm, using e-beam lithography followed by platinum deposition. Next, the gates are capped with a multilayer flake of hexagonal boron nitride (h-BN), transferred *via* polymer-based methods,[22,23] which serves as the gate dielectric. h-BN was chosen here due to its stable performance in contrast to metal-oxides as well as its robustness to electron beam irradiation.[49,50] A layer of PMMA is then spin-coated over the device and irradiated at a spot between the gates by an electron beam. With a dosage of 64 mC/cm^2, a dielectric nanopillar of height 150-200 nm (depending on the PMMA solution concentration and spin speed) remains after the rest of the resist is

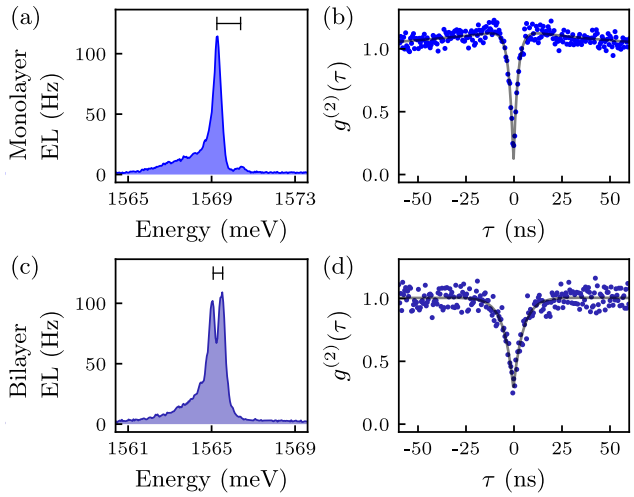

Figure 2: **Demonstration of single photon electroluminescence.** High-resolution EL spectrum of a **(a)** monolayer and **(c)** bilayer WSe_2 device, each showing a single localized exciton doublet with fine structure splittings (denoted by horizontal bars) of 1.1 and 0.5 meV, respectfully. **(b,d)** The second-order autocorrelation functions obtained from the EL in (a,c). Fits using Eq. 1, denoted by gray lines, yield $g^{(2)}(0) = 0.085 \pm 0.029$ for the monolayer and $g^{(2)}(0) = 0.285 \pm 0.034$ for the bilayer.

washed away with solvents.[51] A WSe_2 monolayer is then transferred on top, resulting in a region of high strain in the WSe_2 localized to the junction region (see Section S2 of the Supporting Information (SI) for atomic force microscopy data). Finally, metal anode and cathode contacts (60/5 nm gold/palladium) are created with further lithography and lift-off.

In a completed gate-defined device, the nanopillar strain sites are identifiable as small regions of dark contrast, illustrated for the representative device in Fig. 1b. Thermal annealing after the transfer of the WSe_2 monolayer was found to lead to nanopillar migration away from the junction, which is observable in Fig. 1b. Without the annealing step, minimal migration was observed, reliably yielding devices with strain sites in the junction region. All remaining devices used in this paper were prepared without annealing and measured at a base temperature of 1.6 K, well into the regime where localized exciton emission is prominent.[18] To define the lateral p–n junction, positive and negative voltages were applied to the two gates of a device, creating electron- and hole-rich regions in the overlying monolayer. Then, by applying a current between the anode and cathode contacts, charge carriers are

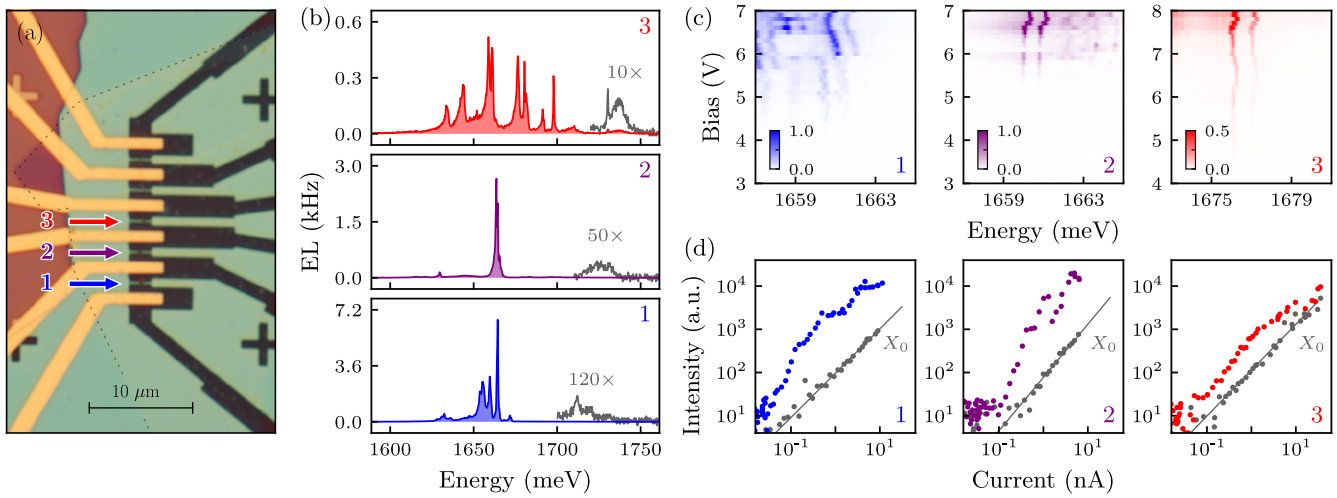

Figure 3: **Deterministic creation of electrically-pumped single photon emitters.** **(a)** Image of a multi-junction monolayer WSe_2 nanopillar device with the three junctions of interest indicated by colored arrows. The nominal diameters of the five nanopillars vary linearly between 300 (bottom) and 100 nm (top). **(b)** Low-resolution EL spectra of the three junctions with injection currents of approximately 4.5 nA and −16 V (12 V) applied to the anode (cathode) gates. The regions around the neutral exciton (X_0) are also shown magnified in gray for each spectrum, highlighting how the SPEs dominate the response. **(c)** Voltage dependence of the EL spectra around one bright doublet per junction. **(d)** Dependence of the integrated intensities (as measured by optical spectroscopy) of the bright doublet (colored) for the three junctions. Lines denote near-linear power law fits to the neutral exciton intensity (gray).

injected into the junction, producing EL.

In Fig. 1c the EL spectrum of a device with a single nanopillar in the junction is shown for an injection current of 4.5 nA. In contrast to the typical low-temperature spectrum of monolayer WSe_2 (also in Fig. 1c) which only exhibits handful of spectrally-broad peaks corresponding to the nonlocalized neutral exciton (X_0) and charged trions (X^-, X^+),[47] the EL of the nanopillar-strained device is dominated by a multitude of bright, narrow-linewidth peaks indicative of individual exciton states localized to the strain site (see Fig. S2 of the SI for EL spatial maps). These range in energy from a few hundred to a few tens of meV below the neutral exciton, overshadowing all nonlocalized emission in that range. With higher resolution spectroscopy, each bright feature can be resolved as a spectral doublet (Fig. 1d): a pair of cross-polarized peaks, separated by a fine structure splitting on the

order of one meV, which undergo correlated spectral wandering (see Section S3 of the SI for further analysis of the doublet structure). This is the signature form of SPEs in TMDs corresponding to localized neutral excitons.[15–19]

To unequivocally confirm that the observed localized exciton states are SPEs, photon autocorrelation measurements were conducted (see Methods). With the use of a narrow linewidth bandpass filter, the EL of a single doublet (Fig. 2a) from a monolayer WSe_2 device was spectrally isolated. The resulting second-order correlation function $g^{(2)}(\tau)$ exhibits clear antibunching at zero time delay ($\tau = 0$), as shown in Fig. 2b. A slight long-timescale bunching is also evident similar to some reported PL measurements.[17,52] To determine the value of $g^{(2)}(0)$, $g^{(2)}(\tau)$ was fit to the phenomenological function describing the exponential recovery of a SPE

$$g^{(2)}(\tau) = 1 - A_1 \exp\left(-\left|\frac{\tau}{t_1}\right|\right) + A_2 \exp\left(-\left|\frac{\tau}{t_2}\right|\right) \quad (1)$$

where A_1 (A_2) and t_1 (t_2) are the antibunching (bunching) amplitude and timescale.[17] This fit yields $g^{(2)}(0) = 0.085 \pm 0.029$, well below the threshold of 0.5 indicative of a SPE.

The fabrication process outlined here isn't restricted to monolayer TMDs; the EL spectra of similar devices based on bilayer WSe_2 were also found to be populated by SPEs which take the spectral form of narrow-linewidth doublets (Fig. 2c-d) but concentrated over a lower range of energies (roughly 1.5 to 1.6 eV[53]) with smaller fine structure splittings. Bilayer devices also exhibit somewhat more favorable electrical characteristics with lower threshold voltages for conduction (see SI Fig. S5).

Prominence of localized exciton emission

The results of the prior section establish how local strain engineering can be used to realize single photon EL from TMDs in a lateral device geometry. In contrast to the vertical devices of Refs. 24–26 which relied on randomly-occurring crystal defects, bright SPE states

are created from lithographically-defined strain sites.[32,33] Similar to the work of Ref. 30, the fabrication process presented here is then in principle deterministic: all devices with a nanopillar in the junction region should exhibit single photon EL. Another noteworthy distinction is that while EL is generated in nearly the entire monolayer TMD area in vertical devices,[24] here it is restricted to the narrow depletion region between the two gates where a high strain gradient enables efficient funneling of carriers into localized exciton states. Consequently uncorrelated emission from nonlocalized excitons – which can compromise the purity of SPEs[5,12] – should be comparatively insignificant.

To demonstrate these qualities, devices were created using a modified design that enables side-by-side testing of multiple nanopillar p–n junctions on a single chip. The main advantage of this device design is that it allows the repeatability of the fabrication process to be easily assessed. One such multi-junction device is shown in Fig. 3a and consists of a WSe_2 monolayer transferred onto five gate-defined junctions, each hosting a single nanopillar. Due to the limited number of electrical connections offered by the measurement system (8 total), only three junctions could be operated at a time. Consequently the analysis is focused on the three bottom junctions (indicated by the colored arrows in Fig. 3a).

In Fig. 3b, EL spectra obtained with approximately the same value of injection current of 4.5 nA are shown for the three junctions. Similar to the device presented in Fig. 1c, bright, narrow-linewidth peaks suggestive of localized excitons dominate the emission in each spectrum. From higher-resolution spectra, the spectral doublet form indicative of SPEs in TMDs can be readily identified (Fig. 3c). Likewise, in a similar device based on bilayer WSe_2, each junction predominately produces SPE EL (see Section S5 of the SI). Together these results confirm the deterministic creation of electrically-pumped single-photon-emitting devices using TMDs.

To compare the intensities of the localized and non-localized emission, EL spectra were collected as a function of the applied bias, focusing on a single bright localized exciton state for each junction (Fig. 3c). These states begin to emit when the bias is increased past the

threshold voltage of roughly 4-5 V (see Fig. S5a of the SI for current-voltage measurements) and increase in intensity, exhibiting no consistent bias dependence of emission energy. Similar to measurements of vertical devices,[25] above the threshold voltage the integrated intensity of each localized state exhibits a sharp rise with increasing injection current followed by a gradual saturation typical of a two-level system (Fig. 3d). In contrast, the neutral exciton emission is markedly lower in intensity and follows an approximately linear dependence throughout the range of currents. Only in the high injection current regime, far after the SPEs begin to saturate, does the nonlocalized emission start to become dominant. At higher currents, these trends are expected to continue but were avoided due to the onset of gate leakage currents at high applied voltages.

The amount of undesirable nonlocalized emission in future devices can in principle be further minimized by taking advantage of two fabrication-level controls. First, by restricting the width of the conducting channel (defined by the underlying gates), the unstrained area in the junction without bright localized exciton states can be minimized. Second, extrapolating from PL studies of TMDs,[32,33] selective design of the strain profile (defined by the nanopillar dimensions) should enable some degree of control over the relative localized and nonlocalized emission. To test this idea for the EL, the diameters of the five nanopillars for the multi-junction device in Fig. 3a were varied linearly from 300 (bottom) to 100 nm (top), thus varying the total amount of strain in each junction. Correspondingly, the neutral exciton peak is less pronounced and lies at a lower energy in junctions with larger nanopillars in accordance with expectations[20,54,55] while the localized exciton emission is brighter (Fig. 3b). While these results are promising, comprehensive characterization similar to the works of Refs. 32,33 is needed to determine the limits of this fabrication-level control of the EL. Through selective modulation of both device geometry and strain, it may be possible to reliably produce devices which emit only from a single SPE state. These would be indispensable for applications in quantum nanophotonics as no spectral filtering would be required to produce purely antibunched emission.[56]

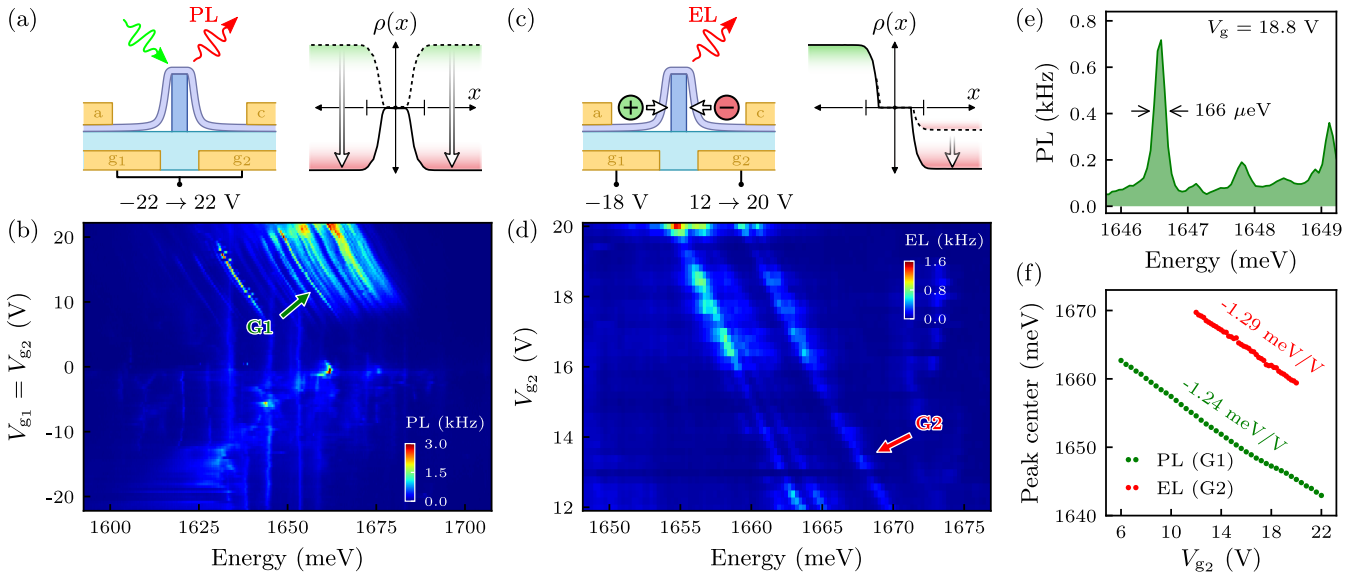

Figure 4: **Tunability of gate-activated localized excitons.** **(a)** Cartoon of unipolar gate-dependent PL measurement. As the gate voltages are increased, the carrier density ρ (calculated following Ref. 43 with a nanopillar of 150 nm height and width) is tuned from the p to n regime with the out-of-plane field following a qualitatively similar functional dependence. Edges of the two gates are marked on the x axis. The dip in ρ near $x = 0$ is due to the decreased gate capacitance for the monolayer region lying on top of the nanopillar. **(b)** The resulting PL spectra for a pump power of 5 μW. The bright feature at 1660 meV with neutral gating conditions is the same doublet from the first panel of Fig. 3c. **(c)** Cartoon of gate-dependent EL measurement. As the cathode gate voltage is increased, the electron density in the junction rises. **(d)** The resulting EL spectra for an injection current of 5 nA. **(e)** High-resolution PL spectrum centered around the peak labeled by the arrow in (b) with 18.8 V applied to both gates. A single Lorentzian fit yields a full width at half maximum of 166 μeV. **(f)** Dependence of the center energy (as obtained from Lorentzian fits) on the applied gate voltage for the peaks labeled by green and red arrows in (b) and (d) respectively.

Gate dependence of localized exciton emission

While the combination of local strain engineering and lateral device geometry enables the reliable creation of devices which predominately emit from SPE states, a distinct advantage of the device structure is that the electrostatic environment can be tuned *in situ via* dedicated gates. As the properties of localized excitons in TMDs are highly sensitive to local fields and charge densities,[19,36–41] selective tuning of the applied gate voltages has the potential to allow active modulation of the emission energies in both PL and EL operation. This is in contrast to vertical devices where only the PL can be modulated.[26,39]

To investigate the degree to which the gate fields influence the emission, PL of the first junction of the device in Fig. 3a was collected over the full range of gate voltages in unipolar operation ($V_{g_1} = V_{g_2}$). This modulates the Fermi level across the junction region, thereby sweeping both the carrier density and out-of-plane electric field over the full range of values (Fig. 4a). As can be seen in Fig. 4b, at zero gate voltage the monolayer is effectively undoped and exhibits the familiar spectral doublets characteristic of localized neutral excitons (Fig. 4b). With the application of positive and negative voltages to both gates, the monolayer becomes populated by charge carriers that enhance Coulomb screening.[57] Consequently, the emission from nearly all localized excitons quenches (the exception being those directly in the center of the junction as can be understood from Fig 4a) and only nominal spectral shifts are observed (see SI Fig. S9 for additional data).

Above a critical positive gate voltage, however, the device enters into a new electrostatic regime marked by the appearance of a large number of bright, narrow-linewidth peaks. Analogous to the spectral doublets at neutral gating conditions, these peaks exhibit sub-meV linewidths (166 μeV for the peak in Fig. 4e) as well as spectral wandering and saturation with pump power (see SI Fig. S7). Dissimilar to neutral conditions, these peaks are only observed to be single peaks with no discernible fine structure splitting with the highest available spectral resolution (Fig. 4e). Together, these findings indicate that the peaks correspond to a new specie of localized excitons distinct from the familiar spectral doublets at neutral doping conditions. To differentiate these states from the localized neutral excitons, they will be referred to as "gate-activated localized excitons" (GALEs).

As the voltage applied to the two gates is increased further, the GALE peaks do not vanish but remain bright and redshift linearly with gate. From a fit to the peak marked in Fig. 4b (G1), a total shift of 19.7 meV over a gate voltage range of 16 V is obtained, yielding a slope parameter of -1.24 meV/V from a linear fit (Fig. 4f). This sizable tuning range is comparable to the largest observed Stark shift of localized neutral excitons in TMDs.[39]

To translate this tunability of the GALE emission to the EL when the device is operated

as a p–n diode ($V_{g_1} < 0 < V_{g_2}$), only the voltage applied to the cathode gate (V_{g_2}) needs to be modulated. This has the effect of tuning the charge density and out-of-plane field in the depletion region close to the cathode gate (Fig. 4c) which, in turn, should modulate the energies of GALE states in that region. In Fig. 4d the experimental realization of this idea is shown, utilizing the third junction of the device in Fig. 3a. With a constant current applied across the junction, a number of GALE peaks can be observed in the EL spectra which redshift in energy as the cathode gate voltage is raised. For the peak marked in Fig. 4d (G2), a total shift of 10.3 meV over a cathode gate voltage range of 8 V is obtained (Fig. 4f). Applying a linear fit yields a slope parameter of -1.29 meV/V, a value that closely matches the corresponding value from the PL measurement. This signifies that the same degree of tunability for the GALE emission has been preserved in switching from optical to electrical pumping.

These results demonstrate the ability for simultaneous electrical pumping and tuning of localized exciton emission from a two-dimensional material. The degree of gate tunability of a GALE state spans a range two orders of magnitude greater than its linewidth (Fig. 4e-f), making it a viable mechanism to correct for the randomness of emission energies *in situ*. Through selective modulation of gate voltages, the EL of a GALE state could be tuned into resonance with a photonic cavity or even the emission from another GALE state. This functionality holds great promise for quantum nanophotonics provided that the GALE states are SPEs. While short-timescale antibunching was observed for the PL of a single GALE peak (see Section S6 of the SI), $g^{(2)}(0)$ was found to lie well above 0.5. This is likely due to the timing jitter of the single photon detectors which can artificially raise the correlation function for SPEs with sub-nanosecond antibunching timescales. Similar to the case of Purcell-enhanced localized exciton emission in TMDs,[58] PL autocorrelation measurements using a pulsed laser source should circumvent this instrument limitation and resolve the statistical nature of the emission but were not viable for this work. Such measurements should also elucidate the physical origin of the GALE states, though the present data do

provide some hints.

From the PL spectra in Fig. 4b, it can be observed that the GALEs appear over an energy range slightly lower than that of localized neutral excitons. Combined with the brightening in response to positive gate voltages, this suggests that the GALEs may be localized negative trions. While these have been observed in gated WSe_2 monolayers, no significant gate-dependent shifting of emission energy has been reported.[36,37] Another exotic possibility lies in the novel coupling between excitons and intervalley plasmons in tungsten-based monolayer TMDs which results in a strongly pronounced sideband in the n-gated regime.[59–61] This quasiparticle, typically labeled $X^{-\prime}$, exhibits similar redshifting and its localization has already been reported in PL measurements of unstrained WSe_2 monolayers with a sub-nanosecond lifetime.[62,63] This interpretation would explain the absence of any reciprocal features in the p-gated regime[59–61] (Fig. 4b) and potentially the multitude of GALE peaks observed as well; since intervalley plasmons enable efficient radiative recombination *via* an intervalley transition, they should permit emission from a greater number of localized exciton states (such as those localized to defects that do not break valley symmetry) which normally are dark.[64] Although the precise origin remains unclear, the control over electrostatic fields in lateral gate-defined devices enables significant tuning of the narrow emission from these localized excitons.

Conclusion

We have demonstrated the creation of gate-defined lateral p–n junctions from monolayer WSe_2 capable of producing single photon EL with local strain engineering. Similar to vertical TMD-based EL devices studied previously,[24–26] the emission spectra are dominated by localized exciton states whose bright, narrow-linewidth peaks show clear photon antibunching. Unlike those devices, however, the use of local strain engineering enables the controllable placement of the SPE states.[30] Combined with the lateral device geometry, this enables the

deterministic creation of p–n junctions which preferentially emit from SPEs. By modulating the electrostatic gating, emission from a novel specie of localized excitons was observed which which exhibits a strongly gate-dependent emission energy. Through selective tuning of the gate voltages, spectral shifts of over 10 meV were induced in the EL, demonstrating simultaneous electrical pumping and tuning of localized exciton emission. These features are critical for scalable control of single photon sources, highlighting a path toward integrating TMD devices into functional quantum optoelectronic devices.

Methods

All measurements were conducted in a closed-cycle cryostat (attocube, AttoDRY2100) at a temperature of 1.6 K unless noted otherwise. A 0.65-mm working distance 100× magnification objective with a numerical aperture of 0.82 (attocube, LT-APO/VIS/0.82) was used collect to luminescence as well as to focus the pump beam (532 nm) in PL measurements.

Optical spectroscopy. Spectroscopic measurements were performed using a 750 mm focal length spectrograph (Andor Shamrock, SR-750) equipped with a thermo-electric-cooled CCD camera (Oxford Instruments, iDUS DU420-A). Depending on the desired spectral resolution, a diffraction grating with either 300 or 1200 lines/mm was used.

Photon autocorrelation. Photon autocorrelation measurements were performed by routing emission to two avalanche photodiodes (PicoQuant, τ-SPAD-100) with a 1×2 fiber splitter in a typical Hanbury Brown-Twiss configuration. To filter out a single SPE state, a 5 nm bandpass filter (Edmund Optics, 39-360 or 39-363) was placed in the beam path and rotated so that its center wavelength matched the emission peak. The second-order correlation function was then obtained using a time-correlated single photon counting module (PicoQuant, HydraHarp 400).

Acknowledgement

Funding sources

This material is based upon work supported by the National Science Foundation under Grant No. DMR-1905986 (2D electronic device) and the Department of the Navy, Office of Naval Research under Grant No. N00014-16-1-3055 (confined emitters). This work made use of the NUFAB and EPIC facilities of Northwestern University's NU*ANCE* Center, which has received support from the SHyNE Resource (NSF ECCS-2025633), the IIN, and Northwestern's MRSEC program (NSF DMR-1720139). K.W. and T.T. acknowledge support from the Elemental Strategy Initiative conducted by the MEXT, Japan (Grant Number JPMXP0112101001) and JSPS KAKENHI (Grant Numbers 19H05790, 20H00354 and 21H05233).

Supporting Information Available

Atomic force microscopy characterization of nanopillar-strained WSe_2 monolayers, analysis of the spectral doublet structure, EL spatial maps, low temperature electrical characterization of monolayer and bilayer WSe_2 *p*–*n* junctions, EL measurements of a multi-junction bilayer WSe_2 device, additional PL measurements of gate-activated localized exciton emission, and additional gate-dependent PL data. This material is available free of charge via the Internet at http://pubs.acs.org

References

(1) O'Brien, J. L.; Furusawa, A.; Vučković, J. Photonic quantum technologies. *Nature Photonics* **2009**, *3*, 687–695.

(2) Gisin, N.; Ribordy, G.; Tittel, W.; Zbinden, H. Quantum cryptography. *Reviews of Modern Physics* **2002**, *74*, 145.

(3) De Martini, F.; Di Giuseppe, G.; Marrocco, M. Single-mode generation of quantum photon states by excited single molecules in a microcavity trap. *Physical Review Letters* **1996**, *76*, 900.

(4) Brunel, C.; Lounis, B.; Tamarat, P.; Orrit, M. Triggered source of single photons based on controlled single molecule fluorescence. *Physical Review Letters* **1999**, *83*, 2722.

(5) Brouri, R.; Beveratos, A.; Poizat, J.-P.; Grangier, P. Photon antibunching in the fluorescence of individual color centers in diamond. *Optics Letters* **2000**, *25*, 1294–1296.

(6) Kuhn, A.; Hennrich, M.; Rempe, G. Deterministic single-photon source for distributed quantum networking. *Physical Review Letters* **2002**, *89*, 067901.

(7) Michler, P.; Kiraz, A.; Becher, C.; Schoenfeld, W.; Petroff, P.; Zhang, L.; Hu, E.; Imamoglu, A. A quantum dot single-photon turnstile device. *Science* **2000**, *290*, 2282–2285.

(8) Kurtsiefer, C.; Mayer, S.; Zarda, P.; Weinfurter, H. Stable solid-state source of single photons. *Physical Review Letters* **2000**, *85*, 290.

(9) Yuan, Z.; Kardynal, B. E.; Stevenson, R. M.; Shields, A. J.; Lobo, C. J.; Cooper, K.; Beattie, N. S.; Ritchie, D. A.; Pepper, M. Electrically driven single-photon source. *Science* **2002**, *295*, 102–105.

(10) Fiore, A.; Chen, J.; Ilegems, M. Scaling quantum-dot light-emitting diodes to submicrometer sizes. *Applied Physics Letters* **2002**, *81*, 1756–1758.

(11) Zinoni, C.; Alloing, B.; Paranthoen, C.; Fiore, A. Three-dimensional wavelength-scale confinement in quantum dot microcavity light-emitting diodes. *Applied Physics Letters* **2004**, *85*, 2178–2180.

(12) Reischle, M.; Beirne, G.; Schulz, W.-M.; Eichfelder, M.; Roßbach, R.; Jetter, M.; Michler, P. Electrically pumped single-photon emission in the visible spectral range up to 80 K. *Optics Express* **2008**, *16*, 12771–12776.

(13) Boretti, A.; Rosa, L.; Mackie, A.; Castelletto, S. Electrically driven quantum light sources. *Advanced Optical Materials* **2015**, *3*, 1012–1033.

(14) Aharonovich, I.; Englund, D.; Toth, M. Solid-state single-photon emitters. *Nature Photonics* **2016**, *10*, 631–641.

(15) Tonndorf, P.; Schmidt, R.; Schneider, R.; Kern, J.; Buscema, M.; Steele, G. A.; Castellanos-Gomez, A.; van der Zant, H. S.; de Vasconcellos, S. M.; Bratschitsch, R. Single-photon emission from localized excitons in an atomically thin semiconductor. *Optica* **2015**, *2*, 347–352.

(16) Srivastava, A.; Sidler, M.; Allain, A. V.; Lembke, D. S.; Kis, A.; Imamoğlu, A. Optically active quantum dots in monolayer WSe_2. *Nature Nanotechnology* **2015**, *10*, 491.

(17) Koperski, M.; Nogajewski, K.; Arora, A.; Cherkez, V.; Mallet, P.; Veuillen, J.-Y.; Marcus, J.; Kossacki, P.; Potemski, M. Single photon emitters in exfoliated WSe_2 structures. *Nature Nanotechnology* **2015**, *10*, 503–506.

(18) He, Y.-M.; Clark, G.; Schaibley, J. R.; He, Y.; Chen, M.-C.; Wei, Y.-J.; Ding, X.; Zhang, Q.; Yao, W.; Xu, X., et al. Single quantum emitters in monolayer semiconductors. *Nature Nanotechnology* **2015**, *10*, 497–502.

(19) Chakraborty, C.; Kinnischtzke, L.; Goodfellow, K. M.; Beams, R.; Vamivakas, A. N. Voltage-controlled quantum light from an atomically thin semiconductor. *Nature Nanotechnology* **2015**, *10*, 507–511.

(20) Kumar, S.; Kaczmarczyk, A.; Gerardot, B. D. Strain-induced spatial and spectral isolation of quantum emitters in mono-and bilayer WSe_2. *Nano Letters* **2015**, *15*, 7567–7573.

(21) Tran, T. T.; Bray, K.; Ford, M. J.; Toth, M.; Aharonovich, I. Quantum emission from hexagonal boron nitride monolayers. *Nature Nanotechnology* **2016**, *11*, 37–41.

(22) Dean, C. R.; Young, A. F.; Meric, I.; Lee, C.; Wang, L.; Sorgenfrei, S.; Watanabe, K.; Taniguchi, T.; Kim, P.; Shepard, K. L., et al. Boron nitride substrates for high-quality graphene electronics. *Nature Nanotechnology* **2010**, *5*, 722–726.

(23) Castellanos-Gomez, A.; Buscema, M.; Molenaar, R.; Singh, V.; Janssen, L.; Van Der Zant, H. S.; Steele, G. A. Deterministic transfer of two-dimensional materials by all-dry viscoelastic stamping. *2D Materials* **2014**, *1*, 011002.

(24) Clark, G.; Schaibley, J. R.; Ross, J.; Taniguchi, T.; Watanabe, K.; Hendrickson, J. R.; Mou, S.; Yao, W.; Xu, X. Single defect light-emitting diode in a van der Waals heterostructure. *Nano Letters* **2016**, *16*, 3944–3948.

(25) Palacios-Berraquero, C.; Barbone, M.; Kara, D. M.; Chen, X.; Goykhman, I.; Yoon, D.; Ott, A. K.; Beitner, J.; Watanabe, K.; Taniguchi, T., et al. Atomically thin quantum light-emitting diodes. *Nature Communications* **2016**, *7*, 1–6.

(26) Schwarz, S.; Kozikov, A.; Withers, F.; Maguire, J.; Foster, A.; Dufferwiel, S.; Hague, L.; Makhonin, M.; Wilson, L.; Geim, A., et al. Electrically pumped single-defect light emitters in WSe_2. *2D Materials* **2016**, *3*, 025038.

(27) Senellart, P.; Solomon, G.; White, A. High-performance semiconductor quantum-dot single-photon sources. *Nature Nanotechnology* **2017**, *12*, 1026.

(28) Liu, X.; Hersam, M. C. 2D materials for quantum information science. *Nature Reviews Materials* **2019**, *4*, 669–684.

(29) Najer, D.; Söllner, I.; Sekatski, P.; Dolique, V.; Löbl, M. C.; Riedel, D.; Schott, R.; Starosielec, S.; Valentin, S. R.; Wieck, A. D., et al. A gated quantum dot strongly coupled to an optical microcavity. *Nature* **2019**, 1–1.

(30) So, J.-P.; Kim, H.-R.; Baek, H.; Jeong, K.-Y.; Lee, H.-C.; Huh, W.; Kim, Y. S.; Watanabe, K.; Taniguchi, T.; Kim, J., et al. Electrically driven strain-induced deterministic single-photon emitters in a van der Waals heterostructure. *Science Advances* **2021**, *7*, eabj3176.

(31) Rosenberger, M. R.; Dass, C. K.; Chuang, H.-J.; Sivaram, S. V.; McCreary, K. M.; Hendrickson, J. R.; Jonker, B. T. Quantum calligraphy: writing single-photon emitters in a two-dimensional materials platform. *ACS Nano* **2019**, *13*, 904–912.

(32) Branny, A.; Kumar, S.; Proux, R.; Gerardot, B. D. Deterministic strain-induced arrays of quantum emitters in a two-dimensional semiconductor. *Nature Communications* **2017**, *8*, 1–7.

(33) Palacios-Berraquero, C.; Kara, D. M.; Montblanch, A. R.-P.; Barbone, M.; Latawiec, P.; Yoon, D.; Ott, A. K.; Loncar, M.; Ferrari, A. C.; Atatüre, M. Large-scale quantum-emitter arrays in atomically thin semiconductors. *Nature Communications* **2017**, *8*, 1–6.

(34) Kok, P.; Munro, W. J.; Nemoto, K.; Ralph, T. C.; Dowling, J. P.; Milburn, G. J. Linear optical quantum computing with photonic qubits. *Reviews of Modern Physics* **2007**, *79*, 135.

(35) Patel, R. B.; Bennett, A. J.; Farrer, I.; Nicoll, C. A.; Ritchie, D. A.; Shields, A. J. Two-photon interference of the emission from electrically tunable remote quantum dots. *Nature Photonics* **2010**, *4*, 632–635.

(36) Brotons-Gisbert, M.; Branny, A.; Kumar, S.; Picard, R.; Proux, R.; Gray, M.; Burch, K. S.; Watanabe, K.; Taniguchi, T.; Gerardot, B. D. Coulomb blockade in an atomically thin quantum dot coupled to a tunable Fermi reservoir. *Nature Nanotechnology* **2019**, *14*, 442–446.

(37) Chakraborty, C.; Qiu, L.; Konthasinghe, K.; Mukherjee, A.; Dhara, S.; Vamivakas, N. 3D localized trions in monolayer WSe_2 in a charge tunable van der Waals heterostructure. *Nano Letters* **2018**, *18*, 2859–2863.

(38) Lu, X.; Chen, X.; Dubey, S.; Yao, Q.; Li, W.; Wang, X.; Xiong, Q.; Srivastava, A. Optical initialization of a single spin-valley in charged WSe_2 quantum dots. *Nature Nanotechnology* **2019**, *14*, 426–431.

(39) Chakraborty, C.; Goodfellow, K. M.; Dhara, S.; Yoshimura, A.; Meunier, V.; Vamivakas, A. N. Quantum-confined Stark effect of individual defects in a van der Waals heterostructure. *Nano Letters* **2017**, *17*, 2253–2258.

(40) Chakraborty, C.; Jungwirth, N. R.; Fuchs, G. D.; Vamivakas, A. N. Electrical manipulation of the fine-structure splitting of WSe_2 quantum emitters. *Physical Review B* **2019**, *99*, 045308.

(41) Mukherjee, A.; Chakraborty, C.; Qiu, L.; Vamivakas, A. N. Electric field tuning of strain-induced quantum emitters in WSe_2. *AIP Advances* **2020**, *10*, 075310.

(42) Xu, X.; Andreev, A.; Williams, D. A. Manipulating quantum-confined Stark shift in electroluminescence from quantum dots with side gates. *New Journal of Physics* **2008**, *10*, 053036.

(43) Massicotte, M.; Vialla, F.; Schmidt, P.; Lundeberg, M. B.; Latini, S.; Haastrup, S.; Danovich, M.; Davydovskaya, D.; Watanabe, K.; Taniguchi, T., et al. Dissociation of two-dimensional excitons in monolayer WSe_2. *Nature Communications* **2018**, *9*, 1–7.

(44) Paur, M.; Molina-Mendoza, A. J.; Polyushkin, D. K.; de Vasconcellos, S. M.; Bratschitsch, R.; Mueller, T. Resonant photocurrent from a single quantum emitter in tungsten diselenide. *2D Materials* **2020**, 045021.

(45) Baugher, B. W.; Churchill, H. O.; Yang, Y.; Jarillo-Herrero, P. Optoelectronic devices based on electrically tunable p–n diodes in a monolayer dichalcogenide. *Nature Nanotechnology* **2014**, *9*, 262.

(46) Pospischil, A.; Furchi, M. M.; Mueller, T. Solar-energy conversion and light emission in an atomic monolayer p–n diode. *Nature Nanotechnology* **2014**, *9*, 257–261.

(47) Ross, J. S.; Klement, P.; Jones, A. M.; Ghimire, N. J.; Yan, J.; Mandrus, D.; Taniguchi, T.; Watanabe, K.; Kitamura, K.; Yao, W., et al. Electrically tunable excitonic light-emitting diodes based on monolayer WSe_2 p–n junctions. *Nature Nanotechnology* **2014**, *9*, 268.

(48) Ross, J. S.; Rivera, P.; Schaibley, J.; Lee-Wong, E.; Yu, H.; Taniguchi, T.; Watanabe, K.; Yan, J.; Mandrus, D.; Cobden, D., et al. Interlayer exciton optoelectronics in a 2D heterostructure p–n junction. *Nano Letters* **2017**, *17*, 638–643.

(49) Wang, J.; Rhodes, D.; Feng, S.; Nguyen, M. A. T.; Watanabe, K.; Taniguchi, T.; Mallouk, T. E.; Terrones, M.; Balicas, L.; Zhu, J. Gate-modulated conductance of few-layer WSe_2 field-effect transistors in the subgap regime: Schottky barrier transistor and subgap impurity states. *Applied Physics Letters* **2015**, *106*, 152104.

(50) Stanev, T. K.; Liu, P.; Zeng, H.; Lenferink, E. J.; Murthy, A. A.; Speiser, N.; Watanabe, K.; Taniguchi, T.; Dravid, V. P.; Stern, N. P. Direct Patterning of Optoelectronic Nanostructures Using Encapsulated Layered Transition Metal Dichalcogenides. *ACS Applied Materials & Interfaces* **2022**, *14*, 23775–23784.

(51) Duan, H.; Zhao, J.; Zhang, Y.; Xie, E.; Han, L. Preparing patterned carbonaceous nanostructures directly by overexposure of PMMA using electron-beam lithography. *Nanotechnology* **2009**, *20*, 135306.

(52) Tripathi, L. N.; Iff, O.; Betzold, S.; Dusanowski, Ł.; Emmerling, M.; Moon, K.; Lee, Y. J.; Kwon, S.-H.; Höfling, S.; Schneider, C. Spontaneous emission enhancement

in strain-induced WSe_2 monolayer-based quantum light sources on metallic surfaces. *ACS Photonics* **2018**, *5*, 1919–1926.

(53) Oreszczuk, K.; Kazimierczuk, T.; Smoleński, T.; Nogajewski, K.; Grzeszczyk, M.; Łopion, A.; Potemski, M.; Kossacki, P. Carrier relaxation to quantum emitters in few-layer WSe_2. *Physical Review B* **2020**, *102*, 245409.

(54) Desai, S. B.; Seol, G.; Kang, J. S.; Fang, H.; Battaglia, C.; Kapadia, R.; Ager, J. W.; Guo, J.; Javey, A. Strain-induced indirect to direct bandgap transition in multilayer WSe_2. *Nano Letters* **2014**, *14*, 4592–4597.

(55) Moon, H.; Bersin, E.; Chakraborty, C.; Lu, A.-Y.; Grosso, G.; Kong, J.; Englund, D. Strain-Correlated Localized Exciton Energy in Atomically Thin Semiconductors. *ACS Photonics* **2020**, *7*, 1135–1140.

(56) Schmidt, R.; Scholz, U.; Vitzethum, M.; Fix, R.; Metzner, C.; Kailuweit, P.; Reuter, D.; Wieck, A.; Hübner, M.; Stufler, S., et al. Fabrication of genuine single-quantum-dot light-emitting diodes. *Applied Physics Letters* **2006**, *88*, 121115.

(57) Hötger, A.; Klein, J.; Barthelmi, K.; Sigl, L.; Sigger, F.; Männer, W.; Gyger, S.; Florian, M.; Lorke, M.; Jahnke, F., et al. Gate-switchable arrays of quantum light emitters in contacted monolayer MoS_2 van der Waals heterodevices. *Nano Letters* **2021**, *21*, 1040–1046.

(58) Iff, O.; Lundt, N.; Betzold, S.; Tripathi, L. N.; Emmerling, M.; Tongay, S.; Lee, Y. J.; Kwon, S.-H.; Höfling, S.; Schneider, C. Deterministic coupling of quantum emitters in WSe_2 monolayers to plasmonic nanocavities. *Optics Express* **2018**, *26*, 25944–25951.

(59) Dery, H. Theory of intervalley Coulomb interactions in monolayer transition-metal dichalcogenides. *Physical Review B* **2016**, *94*, 075421.

(60) Van Tuan, D.; Scharf, B.; Žutić, I.; Dery, H. Marrying excitons and plasmons in monolayer transition-metal dichalcogenides. *Physical Review X* **2017**, *7*, 041040.

(61) Van Tuan, D.; Scharf, B.; Wang, Z.; Shan, J.; Mak, K. F.; Žutić, I.; Dery, H. Probing many-body interactions in monolayer transition-metal dichalcogenides. *Physical Review B* **2019**, *99*, 085301.

(62) Wang, Z.; Mak, K. F.; Shan, J. Strongly interaction-enhanced valley magnetic response in monolayer WSe_2. *Physical Review Letters* **2018**, *120*, 066402.

(63) Muccianti, C. Optical Effects of Excitons in Monolayer Semiconductors. Ph.D. thesis, The University of Arizona, 2021.

(64) Linhart, L.; Paur, M.; Smejkal, V.; Burgdörfer, J.; Mueller, T.; Libisch, F. Localized intervalley defect excitons as single-photon emitters in WSe_2. *Physical Review Letters* **2019**, *123*, 146401.

TOC Graphic

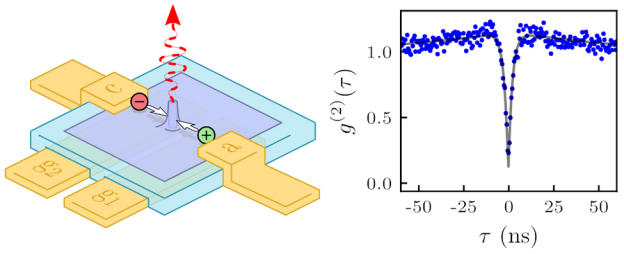

For Table of Contents Only.